Interquinone Electron Transfer in Photosystem I As Evidenced by Altering the Hydrogen Bond Strength to the Phylloquinone(s)

Stefano Santabarbara,*,⊥,†,‡,§ Kiera Reifschneider,† Audrius Jasaitis,‡,§ Feifei Gu,¶,§ Giancarlo Agostini,|| Donatella Carbonera,|| Fabrice Rappaport,‡ and Kevin E. Redding*,†

Department of Chemistry and Biochemistry, Arizona State University, Tempe, Arizona 85287-1604, Institut de Biologie Physico-Chimique, UMR 7141 CNRS-Université Pierre et Marie Curie, 75005 Paris, France, Department of Chemistry, University of Alabama, Tuscaloosa, Alabama 35487, and Department of Chemical Sciences, University of Padua, Via Marzolo 1, 35131 Padova, Italy

Received: April 28, 2010; Revised Manuscript Received: June 5, 2010

The kinetics of electron transfer from phyllosemiquinone ($PhQ^{\bullet-}$) to the iron sulfur cluster F_X in Photosystem I (PS I) are described by lifetimes of ~20 and ~250 ns. These two rates are attributed to reactions involving the quinones bound primarily by the PsaB (PhQ_B) and PsaA (PhQ_A) subunits, respectively. The factors leading to a ~10-fold difference between the observed lifetimes are not yet clear. The peptide nitrogen of conserved residues PsaA-Leu722 and PsaB-Leu706 is involved in asymmetric hydrogen-bonding to PhQ_A and PhQ_B, respectively. Upon mutation of these residues in PS I of the green alga, *Chlamydomonas reinhardtii*, we observe an acceleration of the oxidation kinetics of the $PhQ^{\bullet-}$ interacting with the targeted residue: from ~255 to ~180 ns in PsaA-L722Y/T and from ~24 to ~10 ns in PsaB-L706Y. The acceleration of the kinetics in the mutants is consistent with a perturbation of the H-bond, destabilizing the $PhQ^{\bullet-}$ state, and increasing the driving force of its oxidation. Surprisingly, the relative amplitudes of the phases reflecting $PhQ_A^{\bullet-}$ and $PhQ_B^{\bullet-}$ oxidation were also affected by these mutations: the apparent $PhQ_A^{\bullet-}/PhQ_B^{\bullet-}$ ratio is shifted from 0.65:0.35 in wild-type reaction centers to 0.5:0.5 in PsaA-L722Y/T and to 0.8:0.2 in PsaB-L706Y. The most consistent account for *all* these observations involves considering reversibility of oxidation of $PhQ_A^{\bullet-}$ and $PhQ_B^{\bullet-}$ by F_X, and asymmetry in the driving forces for these electron transfer reactions, which in turn leads to F_x-mediated interquinone electron transfer.

Introduction

Photosystem I (PS I) catalyzes the light-driven oxidation of plastocyanin and reduction of ferredoxin. The majority of the electron transfer (ET) cofactors are bound noncovalently to the PsaA/PsaB heterodimer, which forms the reaction center (RC) and also serves as a core antenna. The only redox-active centers not bound to the PsaA/PsaB heterodimer are the two terminal electron acceptors, the [4Fe-4S] clusters F_A and F_B, which are bound to PsaC.

Phylloquinone (PhQ) acts a secondary electron acceptor. It is reduced in less than 100 ps, and the radical $PhQ^{\bullet-}$ is, in turn, oxidized with polyphasic kinetics by the electron acceptor F_X, a [4Fe-4S] cluster (reviewed in 1–3). A large body of evidence has demonstrated that the two structurally symmetric redox chains, which result from the C_2-symmetric nature of the PsaA/PsaB heterodimer, are both participating in ET reactions.[4–12] However, the two electron transfer branches are not identical and differ in their kinetic properties and their statistical utilization. One such difference relates to the apparent rate of oxidation of the secondary electron acceptor PhQ by F_X. The kinetics of $PhQ^{\bullet-}$ oxidation are described by a minimum of two exponential components, characterized by lifetimes of 10−25 and 200−300 ns, at room temperature.[1,2] On the basis of the effect of site-directed mutants in the PhQ binding sites, the ~250-ns phase of $PhQ^{\bullet-}$ oxidation was attributed to reactions involving the PsaA-bound PhQ (PhQ_A), and the 20-ns phase, to $PhQ_B^{\bullet-}$ oxidation.[4,10–12] The factors that lead to the ~10-fold difference in rate are not fully understood.

According to the crystallographic models,[13,14] the edge-to-edge distance between each PhQ and F_X differ by only fractions of an angstrom, and the orientation of the electron donor and acceptor are virtually identical. Thus, the difference in the oxidation rate of $PhQ^{\bullet-}$ stems from subtle physicochemical properties brought about by protein−cofactor interactions rather than from a purely structural difference. Insight into the factors determining the rate of electron transfer between $PhQ^{\bullet-}$ and F_X has come from investigations of the temperature dependence of the reaction,[15,16] computational studies to estimate the standard redox potential of the PhQ,[17,18] attempts to measure redox potentials by voltammetry,[19] and kinetic modeling based on electron tunneling theory.[2,20] These studies point to a difference of ~40−100 mV between the standard redox potentials of the two phylloquinones, with the $PhQ_B^{\bullet-}/PhQ_B$ redox couple being the more electronegative, making F_X reduction by $PhQ_B^{\bullet-}$ or $PhQ_A^{\bullet-}$ downhill or uphill in energy, respectively.

The redox properties of the PhQ/PhQ^- couple are partly determined by its interaction with the protein matrix, which controls the stability of the semiquinone form. In the case of PS I, the structural models suggest that the keto-carbonyl (position 2) of both PhQ_A and PhQ_B is asymmetrically hydrogen-

* Corresponding authors. (K.E.R.) Phone: +1 480-965-0136. E-mail: Kevin.Redding@asu.edu. (S.S.) Phone: +39 (0)2050314857. Fax: +39 (0)250314815; E-mail: stefano.santabarbara@cnr.it.

† Arizona State University.

‡ Université P. et M. Curie.

§ University of Alabama.

|| University of Padua.

⊥ Present address: Istituto di Biofisica, Consiglio Nazionale delle Ricerche, Via Celoria 26, 20133 Milano, Italy.

¶ Died on July 17, 2007, while working in her postdoctoral lab at the University of Alabama at Birmingham.

10.1021/jp1038656
Published on Web 06/28/2010

bonded. The H-bond donor is the peptide nitrogen of the conserved leucine residues PsaA-Leu722 and PsaB-Leu706. It has been recently shown that substitution of PsaA-Leu722 with tryptophan in the PS I RC of *Synechocystis sp.* PCC 6803 led to effects consistent with weakening of the H-bond to $PhQ_A^{\bullet-}$.[21] Here, we report an investigation of the electron transfer kinetics in PS I of mutants in which these conserved leucines have been replaced with either tyrosine (PsaA-L722Y, PsaB-L706Y) or threonine (PsaA-L722T) in the reaction center of *Chlamydomonas reinhardtii*. (The numbering system used in this article will be the same as in the *Thermosynechococcus elongatus* sequence to allow direct comparison with the crystallographic model.[13]) It is shown that the mutation led to an acceleration of the electron transfer reactions involving either $PhQ_A^{\bullet-}$ (PsaA-L722Y/T) or $PhQ_B^{\bullet-}$ (PsaB-L722Y). Moreover, the fractional amplitudes of the $PhQ^{\bullet-}$ oxidation phases attributed to the reaction involving PhQ_A or PhQ_B are apparently redistributed, in contrast with previous reports for other mutations of the PhQ-binding sites.[4,11,12] We propose an energetic scenario in which the occurrence of interquinone electron transfer, resulting from the low but unequal driving force for electron transfer reactions from $PhQ_A^{\bullet-}$ and $PhQ_B^{\bullet-}$ to F_X, accounts for these observations.

Materials and Methods

Construction and Growth of Mutant Strains. Mutant strains were constructed as previously described.[22] Briefly, the site-directed mutations were constructed by PCR using plasmids designed to reinsert the *psaA-3* or *psaB* genes.[23] Plasmids bearing mutations in *psaA* exon 3 (*psaA-3*) were shot into strains KRC1001-11A (*psaA-3*Δ) and KRC91−1A (*P71 psbA*Δ *psaA-3*Δ), and *psaB* plasmids were shot into strains KRC1000-2A (*psaB*Δ) and KRC94-9A (*P71 psbA*Δ *psaB*Δ), followed by selection for resistance to spectinomycin and streptomycin. All strains were grown under low continuous illumination (∼10 μE m^{-2} s^{-1}) in TAP medium.[24]

Purification of Thylakoid Membranes. Thylakoid membranes were purified by a modification of a previously described procedure.[25] After initial harvesting of membranes as described, they were further purified by a discontinuous (0.1M/1M/2M) sucrose gradient. Excess sucrose was subsequently removed by centrifugation and resuspension in a buffer containing 0.1 M sorbitol, 10 mM NaCl, 5 mM $MgCl_2$, 1 mM $CaCl_2$, and 30 mM Hepes−NaOH (pH 7.8). All purification procedures were performed in either complete darkness or under dim ambient light.

Time-Resolved Optical Spectroscopy. Laser-flash-induced difference absorption kinetics were recorded in whole cells of *C. reinhardtii* using a home-built pump−probe spectrometer[26] as previously described.[12] Cells were harvested by centrifugation during the logarithmic growth phase and immediately resuspended at a concentration giving ∼1 OD_{680} cm^{-1} in a buffer containing Hepes−NaOH (pH 7.0) and 20% w/v Ficoll (Pharmacia), which prevents sedimentation during the measurement. The uncoupler carbonylcyanide-*p*-trifluoro-methoxyphenylhydrazone was added to 10 μM final concentration to prevent the establishment of long-lived transmembrane electrochemical potentials, which give rise to additional electrochromic signals. For each strain, several data sets of absorption-difference transients acquired on different culture batches were globally fitted simultaneously by a sum of exponential functions. The lifetimes were considered only as global parameters, whereas the pre-exponential factors (amplitude) were not globally constrained. The presented decay-associated spectra (DAS) are then obtained by weighted averaging of the DAS resulting from each independent set of measurements. Minimization was achieved by reducing the sum of squared residuals (weighted by the rms noise) by combining an initial search using the Simplex algorithm and a refined minimization using the Levenberg−Marquard algorithm. The software operates in MatLab 7 (The MathWorks, Natick, MA).

Optically Detected Magnetic Resonance. The setup used to record fluorescence detected magnetic resonance (FDMR) and microwave-induced triplet *minus* singlet (T−S) spectra has been previously described in detail.[27] All samples were diluted to a concentration equivalent to 100 μg Chl mL^{-1} in a buffer containing 0.1 M sorbitol, 10 mM NaCl, 5 mM $MgCl_2$, and 60% w/v glycerol immediately before measurement. Prior reduction of PS I electron acceptors was accomplished by a previously described photoaccumulation procedure,[28] with minor modifications. Sodium dithionite was added to the sample (300 μg Chl mL^{-1}) to a final concentration of 11 mM. After a 5-min anaerobic incubation in the dark, samples were diluted into the glycerol-containing buffer, and the sample was illuminated for 5 min with focused white light from a 600-W halogen lamp. Care was taken to minimize the exposure of the samples to light: they were stored on ice in the dark at all times and loaded into the cryostat carefully to avoid exposure to stray light from the excitation source. Deconvolution of the FDMR spectra in terms of Gaussian bands was performed as described.[25,29]

Simulations. The dynamics of the population (molar fractions) evolution of PhQ_A, PhQ_B, and F_X were simulated by the solution of a system of linear differential equations of the form: $d\mathbf{A}/dt = \mathbf{K}\mathbf{A}$, where **A** is the vector of the species and **K** is the rate matrix. The inverse of the eigenvalues of matrix **K** simulated the experimentally measured lifetimes (τ), and the amplitude are given by the eigenvectors solved for the initial conditions, which were kept constant for all the simulations as $PhQ_A^{\bullet-}(0) = 0.5$; $PhQ_B^{\bullet-}(0) = 0.5$; $F_X(0) = 0$. Further details on the calculations are described in ref 2. The elements in the rate constant matrix **K** are calculated using the electron transfer formula derived by Marcus (see reviews of refs 30, 31), corrected for coupling with a mean phonon mode (ϖ) given by Hopfield[32] and DeVault,[31] which has the form:

$$\begin{cases} k_{ET} = \dfrac{2\pi}{\hbar}\cdot|V_{DA}|^2\cdot\dfrac{1}{\sqrt{2\pi\sigma^2(T)}}e^{-(\Delta G^0+\lambda_t)^2/2\sigma^2(T)} \\ \sigma^2(T) = \lambda_t\hbar\bar{\omega}\cdot\coth\dfrac{\hbar\bar{\omega}}{2k_bT} \end{cases} \quad (1)$$

where $\hbar$ is the Dirac constant, k_b is the Boltzmann constant, ΔG^0 is the Gibbs free energy difference at standard conditions, V_{DA} is the electronic coupling element of the Hamiltonian, and $\sigma^2(T)$ is the temperature dependent function describing the width of the Franck−Condon factors. All the measurements were performed at room temperature; hence, we employ the high-temperature approximation and considered $\hbar\varpi = 25$ meV. The value of the donor−acceptor (DA) electronic coupling matrix ($|V_{DA}|$) is determined considering a rectangular potential barrier characterized by a height of 2 eV[31,32] common to all cofactors. This yields a maximal value of $|V_{DA}^0|^2 \simeq 1.5 \times 10^{-3}$ eV^2 at van der Waals contact. An exponential dependence between $|V_{DA}|^2$ and the barrier length is considered customary, which is accounted by the factor $\beta = -1.38$ $Å^{-1}$,[31−33] so that $|V_{DA}|^2 = |V_{DA}^0|^2\cdot e^{-\beta(X_{DA}-3.6)}$. The edge-to-edge distances between the cofactors (X_{DA}), which are assumed to coincide with the barrier lengths, are taken from the *T. elongatus* structure.[13] All calculations were performed in Maple 12 (MapleSoft, Waterloo, Ontario, Canada).

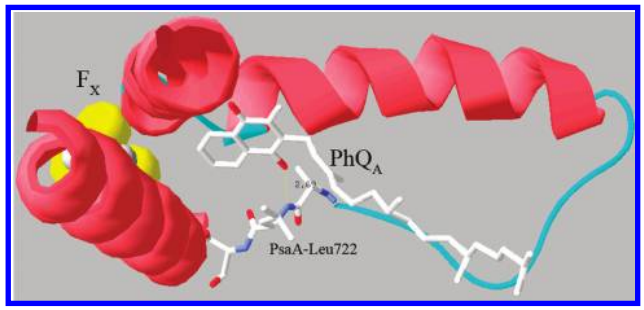

Figure 1. The PhQ_A binding site, seen from "above" the PhQ, with the residue (PsaA-Leu722) targeted in this study (along with the residues immediately before and after) shown as stick figures. Figure made by Swiss-PDBViewer derived from the 2.5-Å crystal structure coordinates of PS I from *T. elongatus* (1JB0[13]). The putative H-bond involving Leu722 and PhQ_A is shown as a dotted yellow line (distance of 2.69 Å).

Results

Mutation of Residues PsaA-Leu722 and PsaB-Leu706: Initial Characterization. To probe the effect of the H-bond to the PhQ on either ET chain, we mutated the Leu residue whose peptide nitrogen acts as donor to the C_2-keto oxygen of PhQ_A (PsaA-Leu722) or PhQ_B (PsaB-Leu706). These were changed to Tyr and Trp on both subunits. Although these mutations should not change the amide directly, the insertion of larger side chains might lead to steric hindrances with the phytyl tail of the nearby PhQ (see Figure 1), in turn perturbing the positioning of the quinone headgroup and its interaction with the protein environment.

Strains lacking either *psaA-3* (third exon of *psaA*) or *psaB* were transformed with plasmids designed to reintroduce the corresponding genes. When transformed with the WT gene, these strains become completely competent for photosynthetic growth.[34] Strains expressing the PsaA-L722W or PsaB-L706W PS I, however, were completely incapable of photosynthetic growth and were almost as light-sensitive as a PS I null strain (data not shown). Immunoblot analysis subsequently demonstrated that their lack of photosynthetic competence was due to extremely low levels of PS I (data not shown). Thus, conversion of the isopropyl group (Leu) to indole (Trp) at this position was not structurally tolerated by the algal protein, although cyanobacterial PS I does tolerate this substitution in the PhQ_A site.[21]

The Leu → Tyr substitutions were much better tolerated. The strain expressing PsaB-L706Y grew normally in heterotrophic

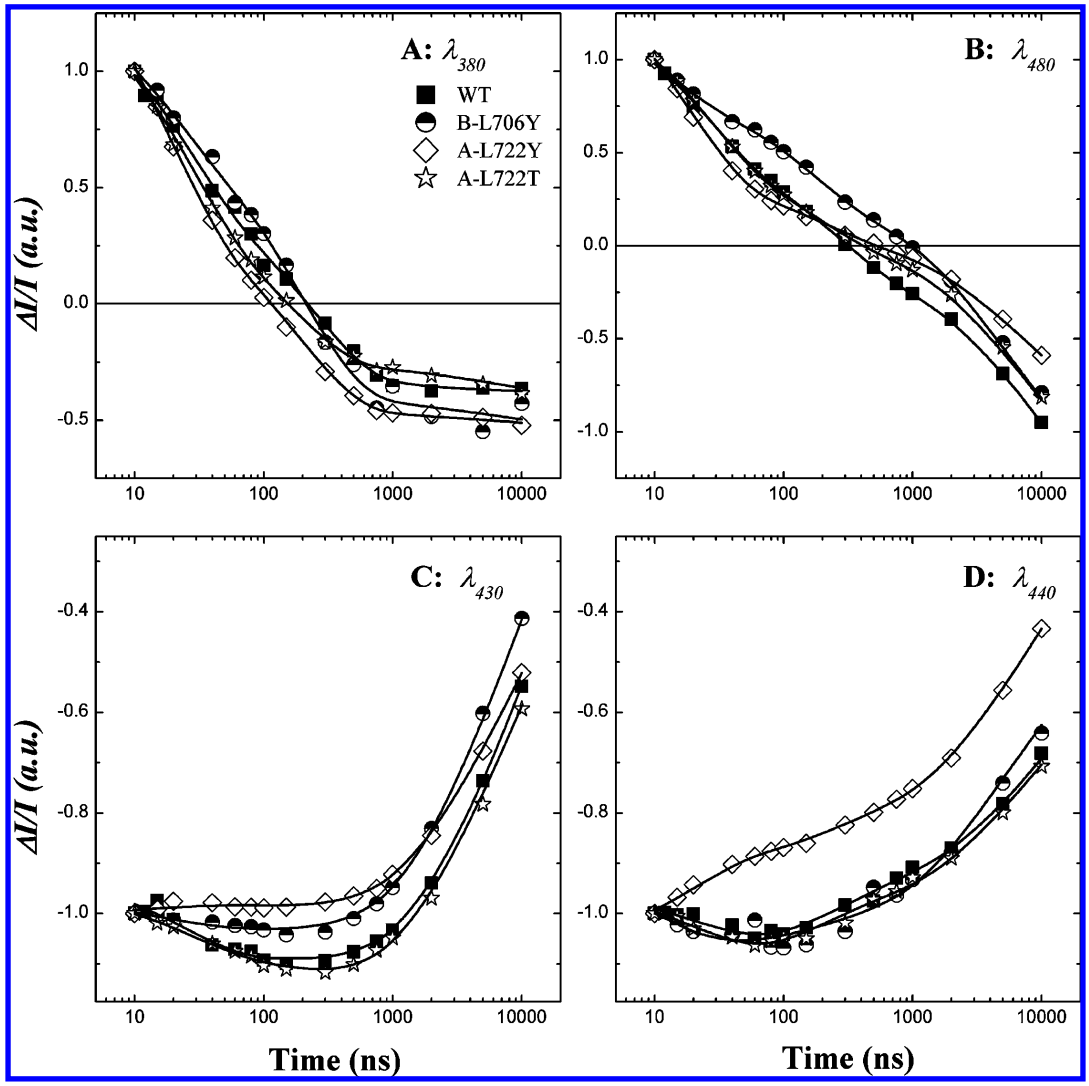

Figure 2. Kinetics of laser flash-photolysis in cells of the WT (■), PsaB-L706Y (°), PsaA-L772Y (◇), and PsaA-L722T (I) mutants of *C. reinhardtii* recorded at different observation wavelengths: 380 nm (A), 480 nm (B), 430 nm (C), and 440 nm (D). Solid lines are the best fits. All the kinetics are normalized on the initial amplitude, but the polarization of the signal (bleach/rise) is maintained.

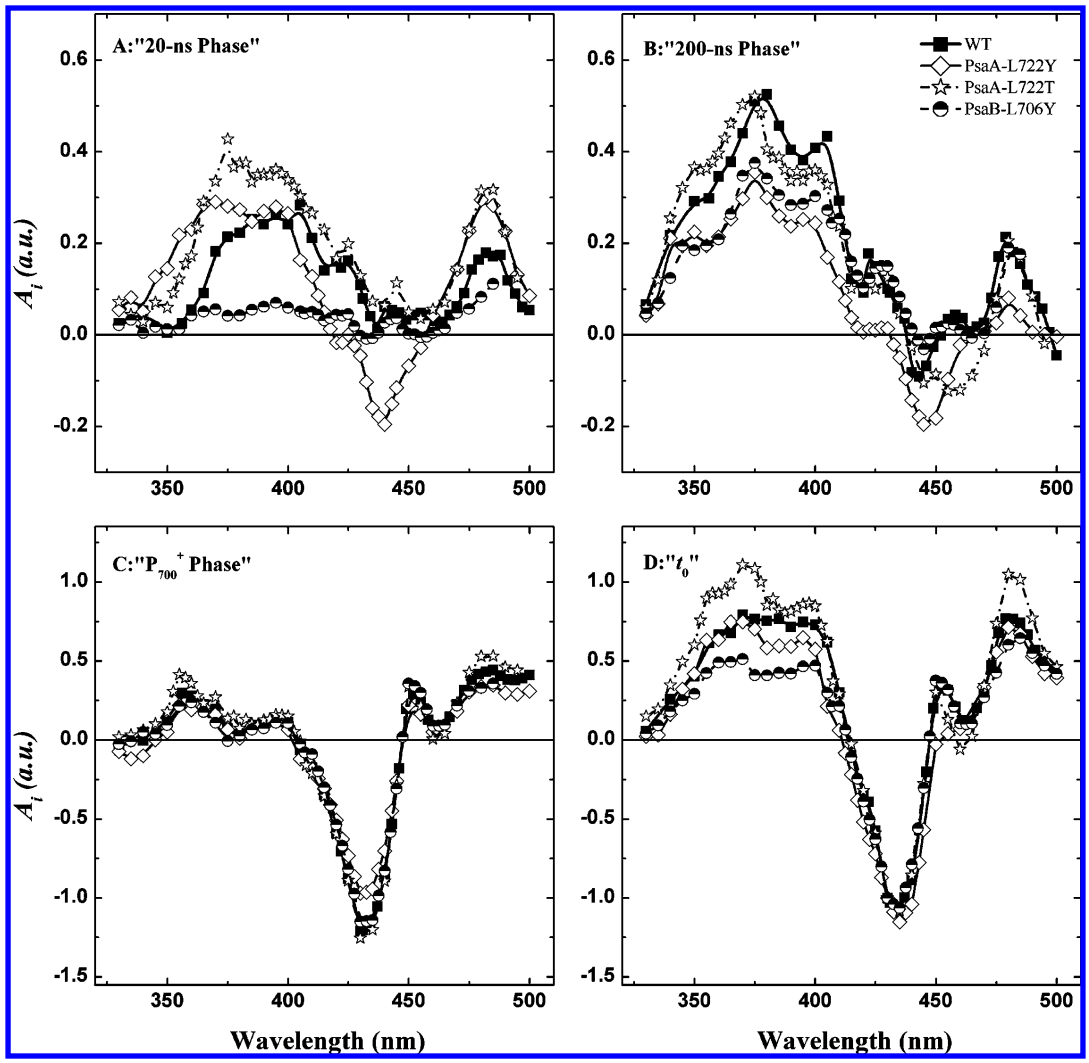

Figure 3. DAS of $\tau_1 = 10-30$ ns (A), $\tau_2 = 150-260$ ns (B), $\tau_3 = 6$ μs. D: Extrapolation at t_0 of the decaying components. Control: thick, solid lines. PsaA-L722Y: open diamonds, dashed lines. PsaA-L722T: open stars, dashed−dotted lines. PsaB-L706Y: solid circles, dotted lines. Spectra were internally normalized on bleaching (430 nm) of the $t = 0$ spectrum.

conditions under low light but grew slightly slower under high light; it was unable to grow photosynthetically under high light (Figure S1 of the Supporting Information). This may be explained by the fact that it contained somewhat less PS I than the WT strain (~35% less), as judged by anti-PsaA immunoblots (Figure S2 of the Supporting Information). The PsaA-L722Y mutant grew poorly in high light, even under heterotrophic conditions (Figure S1 of the Supporting Information), despite the fact that it contained almost the same amount of PS I as the WT control strain (Figure S2 of the Supporting Information).

Given the phenotype of the PsaA-L722Y mutant, we also converted PsaA-Leu722 to Thr in an attempt to make a mutation that was better tolerated. Although the Thr side chain is somewhat smaller than Leu, it seemed possible that the β-branched side chain would introduce steric strain, thus weakening the H-bond from the peptidic amide. The PsaA-L722T mutant grew just as well as the WT strain (perhaps even better; Figure S1) and seemed to have a slightly higher (by ~40%) complement of PS I (Figure S2; Table S1)

To simplify spectroscopic analysis, these mutations were also introduced into a *P71 FuD7* strain (which lacks PS2 and most of the cellular LHC complement). Immunoblot analyses indicated that accumulation of PS I polypeptides in this strain (normalized to total cellular protein) was similar to the WT background strain (data not shown). Subsequent biochemical and spectroscopic work described below was performed with transformants in this genetic background.

Laser-Flash Optical Spectroscopy at Room Temperature: Overview. ET reactions within PS I were monitored by pump−probe spectroscopy in whole cells. The kinetics monitored at selected wavelengths though the absorption spectrum are shown in Figure 2. The data were globally fitted to extract the decay-associated spectra (DAS; Figure 3). In all strains, the kinetics can be fitted satisfactorily by three exponential functions, two of which are characterized by lifetimes in the submicrosecond time-scale, and a nondecaying component (Figure 3). The latter reflects ET reactions involving diffusible electron carriers as well as cytochrome b_6f and is therefore not shown or discussed further. To allow direct comparison of the DAS recorded in the different strains (Figure 3), they have been internally normalized to the maximum bleaching at 430 nm (P_{700}) of the initial spectrum (t_0), which is defined as the sum of the decaying components (within the time range of the experiment), as they reflect ET reactions occurring within the PS I RC.

The two decay components characterized by lifetimes in the submicrosecond time range (Figure 3) are generally assigned to the oxidation of $PhQ^{\bullet-}$ on the basis of their DAS (reviewed

TABLE 1: Fit Parameters Describing the Kinetics of ET in WT and Mutant PS I

	lifetimes[b]			amplitude[c]	amplitude ratio[d]	
	τ_1 (ns)	τ_2 (ns)	τ_3 (μs)	$A_{t0,\lambda 390}$	A_{t0}/A_{t0}^{WT}	A_{τ_1}/A_{τ_2}
control	22 ± 2	256 ± 12	6.2 ± 0.4	0.75	1.00	0.37:0.63
PsaB-L706Y	11 ± 4	197 ± 15	5.7 ± 0.8	0.50	0.66	0.18:0.82
PsaA-L722Y	18 ± 3	205 ± 22	6.4 ± 0.6	0.62	0.83	0.53:0.47
PsaA-L722T	24 ± 2	171 ± 10	6.4 ± 0.3	0.88	1.18	0.51:0.49

[a] Further information reporting values at different wavelengths is presented in Table S2 of the Supporting Information. [b] Lifetimes of the three exponential decay components retrieved from global fitting of ET kinetics in whole cells expressing WT and mutant PS I. [c] The amplitude of the decaying components at 390 nm, extrapolated to time zero (t_0) and normalized to the value at 430 nm. [d] A_{t0}/A_{t0}^{WT} is the amplitude at t_0 (390 nm) normalized to the WT value; A_{τ_1}/A_{τ_2} is the (normalized) ratio of the fast to slow component at 390 nm.

in 1 and 2). However, as seen in Figure 3, the DAS of the ~20-ns and ~250-ns components recorded in the WT, PsaA-L722, and PsaB-L706 mutated strains display significant differences, in terms of both band shape and amplitude. In contrast, the DAS of the ~5-μs components, assigned to the reduction of P_{700}^+ by prebound plastocyanin,[35,36] are similar in shape and amplitude in all strains (Figure 3), with the exception of the PsaA-L722Y mutant, which exhibits slightly smaller amplitudes around 430 nm (discussed in more detail below).

Phyllosemiquinone Oxidation in the Mutants: Lifetimes. In the wild-type (WT) control strain, the rapid $PhQ^{\bullet -}$ oxidation phase is characterized by a lifetime of 22 ± 2 ns, and the slower phase, by a lifetime of 256 ± 12 ns (Table 1), in agreement with previous reports (e.g.,[4,10–12]). The submicrosecond kinetics recorded in the PsaA-L722Y mutant can be globally described by lifetimes of 18 ± 3 ns, which is similar to that detected in WT, and 205 ± 22 ns, which is slightly smaller. Similarly, in the PsaA-L722T strain, the two submicrosecond components have lifetimes of 24 ± 2 ns and 171 ± 10 ns. Although the lifetime of the faster component is similar to the control, the slower nanosecond phase is significantly shorter. In the PsaB-L706Y strain, the lifetimes of the submicrosecond components are also accelerated: 11 ± 4 and 197 ± 15 ns. Thus, in the three mutants, at least one of the two submicrosecond components was slightly but significantly accelerated, and the interpretation of this acceleration requires scrutiny of the DAS (Figure 3).

Phyllosemiquinone Oxidation in the Mutants: DAS. ***PsaB-L706Y.*** The DAS of the fast 10-ns component has very weak amplitude throughout the spectral region investigated, particularly in the UV (~10% of WT value at 390 nm; Figure 3). Thus, the 197-ns component dominates the decay in the nanosecond time window. With respect to the control, the ratio between the faster and slower components (in the 380−390 nm region) is shifted from 0.37:0.63 to 0.18:0.82 (Table 1). The amplitude for the DAS assigned to P_{700}^+ reduction (Figure 3) is similar to that of the control, indicating that there is no significant amount of fast back-reaction in the mutant PS I. Despite this, the amplitude of the t_0 spectrum in the $PhQ^{\bullet -}$ absorption region (365−400 nm) is decreased by 35−45% as compared with the control (Figure 3, Table 1). This stems primarily from the decreased amplitude of the fast (10-ns) decay component, although a slight decrease in the slow (197-ns) phase is observed, as well.

PsaA-L722T. The spectra of both the fast and slow phases of $PhQ^{\bullet -}$ oxidation differ from the control in several respects. The shape and the amplitude of the DAS of the slower (171-ns) component in the near UV, which is dominated by $PhQ^{\bullet -}$ absorption, is very similar to that of the control, except for a slight blue shift and the relative increase in amplitude of the shoulder located at 350 nm (Figure 3). However, it also displays negative amplitude between 440 and 470 nm, with a broad and more pronounced minimum between 445 and 458 nm, as compared with the control. The position and the intensity of these spectral features resemble those of the so-called "intermediate" phase, which has a similar lifetime (~180 ns) and was assigned to ET from F_X^- to $F_{A/B}$.[11,12]

The DAS of the fast (24-ns) component is very similar to that of the control strain at wavelengths longer than 370 nm, but its overall intensity is increased by ~15−20% (Figure 2A). At wavelengths shorter than 380 nm, the increase in the intensity of the signal in the PsaA-L722T strain is conspicuous. As a consequence, the ratio between two kinetic phases of $PhQ^{\bullet -}$ oxidation is close to 0.5:0.5 on average, estimated by monitoring either the $PhQ^{\bullet -}$−PhQ absorption difference (360−400 nm) or the electrochromic band-shift (ECS, 470−520 nm). Moreover, after normalization to the maximum bleaching at 430 nm, the differential absorption in the near-UV region extrapolated to t_0 shows a ~15−20% increase as compared with WT (Figure 3, Table 1).

PsaA-L722Y. Much more dramatic differences in spectral shape are observed in the PsaA-L722Y mutant. The DAS of both the 18-ns and 205-ns components display a pronounced local minimum at 440−460 nm. Similar spectral features were previously observed in the PsaA-M684H mutant of *C. reinhardtii*.[11] On the basis of the bleaching position and the apparent lifetime, this spectral feature was assigned to charge recombination from the $[P_{700}^+A_0^-]$ radical pair (reviewed in 37). In the near-UV region, the DAS of the 205-ns component is similar to that recorded in the control strain, but for a decrease in amplitude. The DAS of the 18-ns component is close in amplitude to that of the WT at wavelengths longer than 375 nm, but it displays a pronounced amplitude increase between 350 and 370 nm. As a result, the relative ratio between the rapid and slow phases of $PhQ^{\bullet -}$ oxidation, as monitored in the 380−390 nm range, is shifted to values near ~0.5:0.5 (Table 1). This redistribution in the relative amplitude of the $PhQ^{\bullet -}$ oxidation phases is even more pronounced around 480 nm (ECS; Figure 3), but this effect is likely due to the profound alteration of the DAS band shape in this spectral region brought about by the occurrence of charge recombination events (see below).

Finally, we observed a moderate decrease of the amplitude of the t_0 spectrum in the near-UV region (10−15%; Figure 3). At the same time, the DAS associated with P_{700}^+ reduction (6.4 ± 0.6 μs) also has ~15% lower amplitude than the control (Figure 3), which is indicative of P_{700}^+ being reduced by events faster than the microsecond time scale (e.g., charge recombination; see below). Thus, in the PsaA-L722Y mutant, the ratio between stable (on the submicrosecond time scale) P_{700}^+ oxidation and PhQ reduction is substantially the same as in the control. Nevertheless, the apparent redistribution of amplitude from the slower component to the faster one remains valid, as this is independent of the choice of internal normalization.

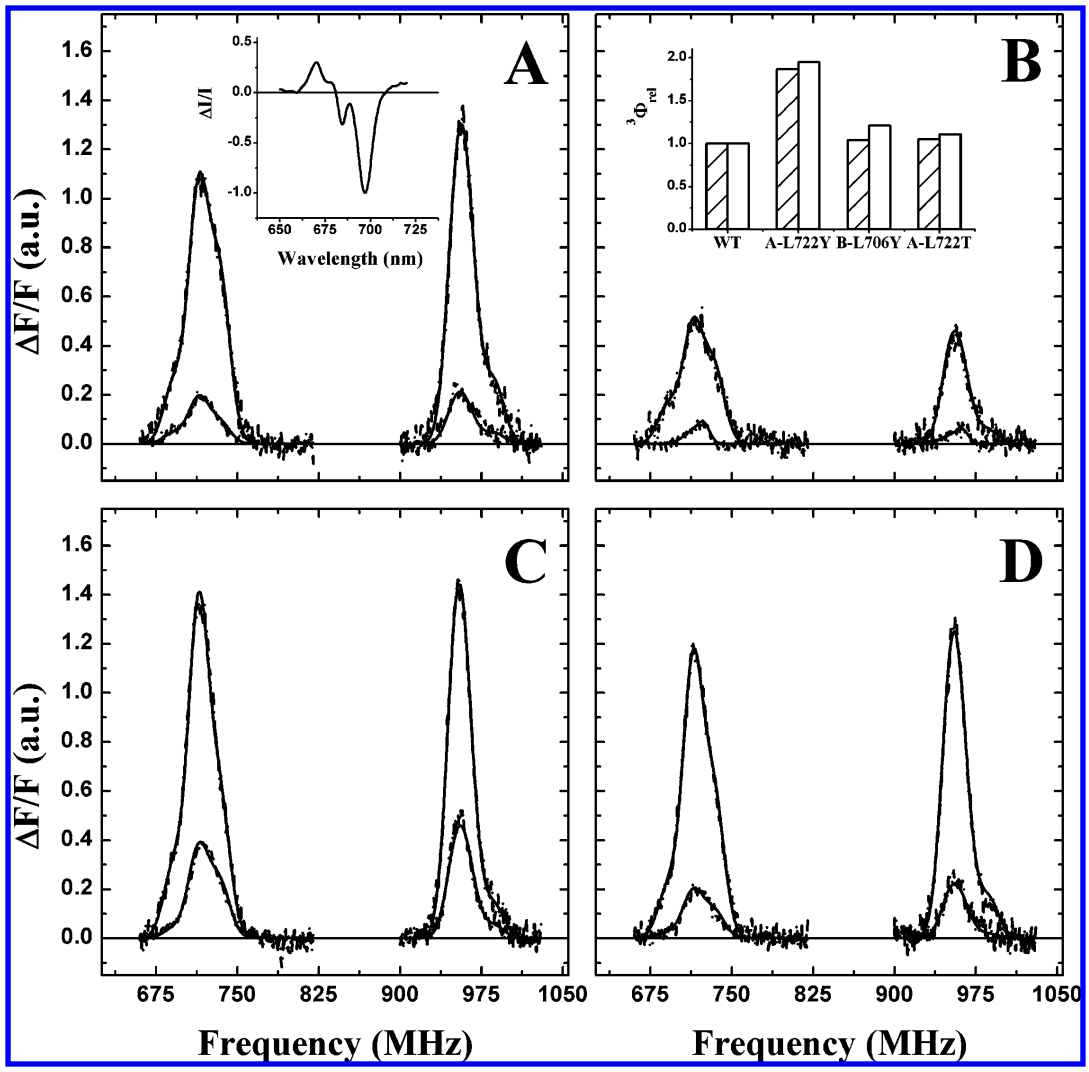

Figure 4. FDMR spectra recorded in isolated thylakoids from *C. reinhardtii* strains expressing WT (A), PsaB-L706Y (B), PsaA-L722Y (C), and PsaA-L722T (D) PS I, either under ambient redox conditions or following illumination at RT in the presence of dithionite. Experimental conditions: $T = 1.8$ K; emission wavelength, 720 nm; modulation amplitude, 33 Hz. Inset in panel A is the triplet-minus-singlet spectrum in the control (pump 955 MHz; see Figure S5 for the mutants). Inset in Panel B exhibits the relative $\Phi^3_{P_{700}}$ yields computed by considering all detected triplets (hollow bars) or after discarding the 687/997 MHz population (hatched bars). All values are normalized to that of the WT ($\Phi^3_{P_{700},WT} \equiv 1$).

PsaA-L722Y and PsaB-L706Y Mutants: $^3P_{700}$ Yield at 1.7 K. The transient optical measurements in the PsaA-L722Y mutant at room-temperature were consistent with the occurrence of charge recombination from the $[P_{700}^+A_0^-]$ radical pair, which should lead to population of the P_{700} triplet state ($^3P_{700}$).[37] To test this hypothesis, the steady-state population of $^3P_{700}$ was monitored by FDMR, which allows selective detection of triplet states. A drawback of FDMR detection is that absolute quantification of the triplet yield is not possible (see discussion in refs 25 and 29). This may be overcome, however, by taking the intensities of the FDMR transitions in samples with fully reduced PhQ as internal normalization standards.[28]

The FDMR spectra of thylakoid membranes purified from the control and mutant strains were monitored at 720 nm, either in samples incubated with dithionite in the dark or following preillumination in the presence of dithionite at ambient temperature (Figure 4). Brief incubation in the presence of dithionite was previously shown to affect neither the intensity nor the band-shape of FDMR signals in thylakoid membranes.[29] All the samples displayed resonance transitions with maxima at ~725 MHz (|D| − |E|) and ~955 MHz (|D| + |E|). However, the resonance profiles exhibited somewhat different band shapes and intensities in the strains investigated. The intensities of the FDMR signals ($\Delta F/F$) recorded after photoaccumulation were similar in all the strains, except for the PsaB-L706Y mutant (Figure 4). The weakness of the FDMR signal in PsaB-L706Y thylakoids appears to be correlated with weaker steady-state emission from this sample, which was ~10-fold less than in all other sample investigated (data not shown). Thus, to quantify more reliably the relative $^3P_{700}$ yields ($\Phi^3_{P_{700}}$) in the mutant strains with respect to the control, the FDMR spectra were globally deconvoluted as Gaussian bands (see Figures S3 and S4 of the Supporting Information).

The FDMR spectra are described by three triplet populations (Table 2), which have maxima at 687/997, 719/948, and 746/963 MHz. The triplets showing larger intensity have resonances at 719/948 MHz and 746/963 MHz and are assigned to $^3P_{700}$ on the basis of their |D| and |E| values[25,28,29,38] and on the associated microwave-induced triplet *minus* singlet spectrum (inset of Figure 4A; Figure S5). The 687/997 MHz triplet population has been previously observed in thylakoids isolated from WT *C. reinhardtii* and was assigned to the outer antenna triplet.[25] However, it is also observed in the low antenna background strain, and contrary to the previous report,[25] it responds to the redox state of PS I acceptors (Figure 4; see also Figures S3, S4). Since the assignment of this triplet is

TABLE 2: Global Gaussian Decomposition of FDMR Spectra: Fit Parameters

	|D|-|E| (MHz)	|D|+|E| (MHz)	|D| (cm^{-1})	|E| (cm^{-1})	assignment
T_1	719.4 ± 0.5	948.1 ± 0.5	0.0278	0.0038	$^3P_{700}$
T_2	746.0 ± 0.5	963.1 ± 0.5	0.0285	0.0038	$^3P_{700}$
T_3	687.0 ± 0.5	996.5 ± 0.5	0.0281	0.0052	$^3P_{700}$/core red forms

Best global-fit parameters for the centre frequencies and the width of Gaussian functions describing the FDMR spectra of the |D| − |E| and the |D| + |E| resonances in the wild-type and the PsaA-L722 and PsaB-L706 mutants of *C. reinhardtii*. Also indicated are the ZFS parameters |D| and |E| (errors ±0.0001 cm^{-1}).

somewhat ambiguous, the quantification of $\Phi^3_{P_{700}}$ (inset of Figure 4B) was performed either neglecting (dashed bars) or taking into account (hollow bars) the 687/997-MHz band. In any case, its contribution is quite small and does not impact the conclusions drawn.

In thylakoid membranes from the PsaA-L722T mutant, $\Phi^3_{P_{700}}$ is increased less than ∼5% with respect to the control, an amount that is within the uncertainty of the procedure. In contrast, $\Phi^3_{P_{700}}$ is doubled in the PsaA-L722Y mutant (Figure 4B, inset). In the PsaB-L706Y mutant, $\Phi^3_{P_{700}}$ is increased by ∼20−25%, which falls just outside the uncertainty of this measurement. However, the overall signal intensity of triplets in thylakoids isolated from this strain was particularly low (from two independent thylakoid preparations; see Figure 4B). At present, we are unable to account fully for this observation. Nevertheless, the low FDMR signal in PsaB-L706Y is associated with weak steady-state PS I emission between 710 and 740 nm (data not shown). This might arise, for example, from the significant quenching of fluorescence emission in this strain, which would, in turn, lower the absolute $\Phi^3_{P_{700}}$. The molecular mechanism at the origin of such a process requires further investigation, which is outside the scope of this work. Hence, we suspect that $\Phi^3_{P_{700}}$ yields might be somewhat overestimated in this strain. Nevertheless, we can state with confidence that the increase in $\Phi^3_{P_{700}}$ in the PsaB-L706Y mutant strain is markedly less pronounced than in PsaA-L722Y.

Discussion

Bidirectional Electron Transfer. Mutations of PhQ_A and PhQ_B binding sites have been instrumental in elucidating the involvement of both phylloquinones in ET reactions within PS I (reviewed in refs 2, 39, and 40). Mutation of either PsaA-Trp697 or PsaB-Trp677, which are π-stacked to the aromatic ring of PhQ_A or PhQ_B, led to a specific retardation of the ∼20-ns component (PsaB-W677F) or the ∼250-ns component (PsaA-W697F), respectively.[4] The amplitudes of the two reoxidation phases were not observed to change significantly in the mutants. Mutations of other residues in the vicinity of the PhQ_A[11,39,41] or PhQ_B[39,42] cofactors similarly affected the lifetimes but not the amplitude of the corresponding component. In contrast, the amplitudes of the ∼20-ns and ∼250-ns components were shown to be redistributed in mutants affecting the properties of the ec3 Chl (alternatively labeled as A_0) located directly upstream in the ET chain.[10,11] Moreover, the specific effects of the mutations of the $ec3_A$ and PhQ_A binding sites were shown to be additive.[12] These results fit nicely into a simple model in which the measured lifetimes of ∼250 ns and ∼20 ns represent the actual kinetic constant of $PhQ_A^{\bullet-}$ and $PhQ_B^{\bullet-}$ oxidation, respectively. The fractional amplitude would then be determined solely by the partitioning of charge separation between the A and B branches, irrespective of the detailed mechanism of charge separation (see refs 2, 40, 43, and 44 for detailed discussions of this issue).

Substitution of the Leu residue involved in H-bonding to PhQ_A led to an apparent acceleration of the slow phase of $PhQ^{\bullet-}$ oxidation, from 256 ± 12 ns to 205 ± 22 ns in the PsaA-L722Y mutant or to 171 ns in the PsaA-L722T mutant. The lifetime of the fast $PhQ^{\bullet-}$ oxidation remained substantially unchanged (18 ± 3 ns). In contrast, the fitted lifetime of the rapid oxidation phase was accelerated ∼2-fold in the PsaB-L706Y strain, while the lifetime of the slow phase displayed a less pronounced decrease to 197 ns.

Interestingly, in both the PsaA-Leu722 and PsaB-Leu706 substitution mutants, the affected rates are faster than observed with WT RCs, but in all previously examined *Chlamydomonas* PS I mutants the oxidation kinetics were slower (reviewed in refs 2 and 39). Although their amplitudes differed from WT, the DAS of the fast and slow components in the mutants examined here retained the spectroscopic features characteristic of $PhQ^{\bullet-}$ oxidation (i.e., $PhQ^{\bullet-}$ absorption in the near-UV and ECS in blue-green region). Although we cannot exclude additional contributions from successive ET steps (see, e.g., refs 11, 12, and 16), the different absorption signals in the UV are dominated by the $PhQ^{\bullet-}$ oxidation reactions, and so are the associated kinetics.

An increase in the effective rate for a reaction can be explained by classical ET theory in more than one way,[30,31] but we think it is unlikely that the point mutations we have introduced result in a significant change in either the $PhQ-F_X$ distance or in the reorganization energy of the ET reaction. Thus, it seems likely that the mutations exert their effect by increasing the driving force. Breaking or weakening the H-bond to PhQ should destabilize the semiquinone form, leading to a more electronegative reduction potential for the $PhQ/PhQ^{\bullet-}$ pair and a larger driving force for the oxidation of $PhQ^{\bullet-}$ by F_X, provided the standard midpoint potential of the latter is not much affected by the mutations.

Perturbation of H-bonding to PhQ_A has been reported for the PsaA-L722W mutant of *Synechocystis* sp. PCC6803,[21] on the basis of the alteration of methyl-H hyperfine couplings affecting the spin-polarized EPR spectrum. This investigation was performed at 77 K, a temperature at which forward electron transfer from PhQ_A to F_X is largely blocked, precluding analysis of ET kinetics in the mutant; however, transient experiments done at 240 K were consistent with a significant acceleration of forward ET from PhQ_A in this mutant.[45] If the H-bond to the quinone were also weakened in the PsaA-L722Y/T and PsaB-L706Y mutants, it would account for the experimental trend in kinetics observed here. It should be stressed that the H-bond donor is the amide nitrogen of PsaA-Leu722 and, thus, cannot be eliminated (except, perhaps, by conversion to Pro). However, inclusion of bulkier (such as Tyr or Trp) or β-branched (such as Thr) side chains might lead to steric hindrance that alters the PhQ binding. In turn, this could lead to weakening of the H-bond strength and perhaps also reduction of the affinity of the binding site for PhQ.

Nonfunctional PhQ_A Sites in the PsaA-L722Y Mutant. We found that a certain fraction of PhQ_A sites seemed to be inactive in the PsaA-L722Y mutant. The trough in the 440−450 nm range in the DAS of the two submicrosecond components,

together with the increased triplet yield, indicate that charge recombination from the $[P_{700}^{+}A_0^{-}]$ radical pair is occurring in a fraction of PS I RCs in this mutant. Moreover, the amplitude in the phyllosemiquinone region of the DAS (365−400 nm) was diminished for the slower component, but not the faster one. This effect was bigger in the PsaA-L722Y mutant than it was in the Psa-L722T mutant, arguing that it was not due merely to a change in the kinetics of PhQ_A reoxidation, because the increase in the rate of this reaction was, if anything, larger in the latter. Taken together, it would seem that some fraction of PhQ_A sites are unable to serve as electron acceptors from the $ec3_A$ chlorophyll, leading to a subsequent back-reaction from $P_{700}^{+}ec3_A^{-}$ and generation of $^3P_{700}$.

We can envision two ways in which a PhQ_A site could be inactivated by the mutation. In the first, the nonfunctional sites may be unoccupied, due to a mutation-induced decrease in affinity for phylloquinone. In the second hypothesis, the nonfunctional sites are occupied by doubly reduced phylloquinone (phylloquinol). The latter has been advanced to explain the loss of the photoaccumulated $PhQ_A^{\bullet-}$ EPR signal in the PsaA-L722W mutant of *Synechocystis* sp. PCC6803,[21] and the authors of that paper suggested that the H-bond from the amide of PsaA-Leu722 may normally prevent protonation of the associated phylloquinone, thus inhibiting full reduction to phylloquinol. At this point, we cannot exclude either possibility, and it remains possible that both may occur to some extent. However, we must note that the experimental conditions used here significantly differ from the study of Srinivasan et al,[21] since the kinetics were acquired in whole cells without addition of redox mediators. Thus, if double-reduction were the reason for inactive sites, these sites must have had phylloquinol from the beginning, after growth in low light. Moreover, they would have had to maintain the same proportion of phylloquinol-occupied sites throughout the experiment. These typically last for several hours, during which time the cells are maintained in the dark and only see one single-turnover flash every few seconds or more. The steady-state proportion of phylloquinol-occupied sites would be a function of the rates of double-reduction and phylloquinol/phylloquinone exchange, and it seems unlikely that they could have maintained such a high fraction of phylloquinol at such a low turnover frequency. Preliminary experiments with whole cells of the PsaA-L722Y mutant to quantify loss of stable P_{700} photobleaching (by inducing back-reaction) after varying times of high illumination have not provided evidence for increased inactive sites (data not shown).

Lastly, although sodium dithionite was employed in our FDMR experiments, care was taken to minimize the exposure of thylakoids to the even weak ambient light before freezing. The estimate of inactive sites in the PsaA-L722Y mutant was not higher by this method than obtained by the kinetics in whole cells, arguing against double-reduction occurring in the membranes *in vitro*. The first hypothesis (lowered affinity for phylloquinone in the PhQ_A site) seems to explain the data better because the proportion of empty sites would be a function of the equilibrium of phylloquinone partitioning between "free" quinone in the membrane, which is likely quite low,[46] and would thus remain relatively constant in whole cells and membranes. One might, however, expect the amount of empty sites to increase in purified particles, where free phylloquinone would be absent, and we are currently testing this possibility.

Although the presence of a fraction of PS I with an empty (or double-reduced) PhQ_A site seems to apply to the PsaA-L722Y mutant, it cannot account for the results obtained in the PsaA-L722T mutant, since neither the DAS of the submicrosecond components nor the FDMR data provide evidence for charge recombination in this mutant. Incidentally, if one assumes that a weakened H-bond to PhQ_A explains the faster kinetics in both mutants, then this would provide another argument against the hypothesis of double-reduction of phylloquinone because the effect on kinetics is stronger in the PsaA-L722T mutant, and it would thus be expected to have a weaker H-bond than in the PsaA-L722Y mutant and, thus, more double-reduction of PhQ_A. Conversely, the bulkier Tyr residue at position 722 would be expected to produce a larger steric clash with the phytyl tail of PhQ_A than the smaller Thr side chain, giving rise to a larger proportion of empty sites. The observed changes in the initial difference spectrum and the relative amplitudes of the fast and slow phases of $PhQ^{\bullet-}$ oxidation in the PsaA-L722T mutant must therefore stem from a different process. Thus, even though the results presented in this study provide additional support for the functionality of both ET chains in PS I, in that mutations in the PhQ_A site affect principally the slower kinetic component of $PhQ^{\bullet-}$ oxidation and mutations in the PhQ_B site affect principally the faster one, these results challenge some aspects of the commonly accepted model of ET reactions in PS I discussed above.

Stoichiometry of P_{700} Oxidation and PhQ Reduction. The initial difference spectrum (sum of the decaying components extrapolated to t_0) reflects the total transient absorption changes associated with ET events occurring within the RC immediately after the excitation, at least within our temporal resolution (∼5 ns). In this spectrum, one expects contributions predominantly from $[P_{700}^{\bullet+}-P_{700}]$ and the two $[PhQ^{\bullet-}-PhQ]$ difference spectra because those are the species possessing large differential extinction coefficients in the spectral range examined. When ET from A_0 is significantly slowed down or when charge recombination takes place, the $[A_0^{-}-A_0]$ difference spectrum will also contribute to the initial spectrum. The DAS presented in Figure 3 (panels C) indicate identical relative levels of P_{700} oxidation for all strains, except in the case of PsaA-L722Y. Thus, a similar amount of negative charge (i.e., $PhQ^{\bullet-}$) should be observed in the other strains, leading to an identical extrapolation for the spectra at t_0 in the UV region. This expectation was not always met.

In the PsaB-L706Y mutant, the initial difference spectrum is decreased by over 30% throughout the $[PhQ^{\bullet-}-PhQ]$ spectral region (340−410 nm; see Figure 3D, Table 1). A less pronounced decrease in amplitude is also visible at wavelengths longer than 470 nm, in the ECS region. These effects are largely due to decreased amplitude of the fast phase (∼10 ns), which displays less than 25% the intensity of the corresponding kinetic component (∼20 ns) in WT PS I (Figure 3, Table 1). The most likely explanation for this observation is related to a significant increase in the rate of ET from PhQ_B to F_X (i.e., on the order of a few ns). The increased rate could be a direct effect of perturbing the H-bond, thereby leading to an increased driving force, as discussed above. At the same time, the loss in the initial signal amplitude would be purely apparent, as much of the decay would simply fall within the instrument dead time. As a consequence, the fitted lifetime of 11 ± 4 ns likely represents a substantial overestimate of the actual time-constant, as only the "tail" of the kinetics would be observed by our measurements.

The PsaA-L722T mutant displayed the opposite behavior, in that the amplitude of the $[PhQ^{\bullet-}-PhQ]$ contribution to the initial spectrum was larger than in WT PS I. This was also unexpected. This is largely brought about by an increase in the amplitude

of the 24-ns oxidation phase, whereas the amplitudes of the accelerated 171-ns component and P_{700}^+ reduction are virtually the same as in WT (Figure 3). This also results in an apparent redistribution of the utilization of PhQ_A and PhQ_B from a value of ~2:1 in the control to a value of ~1:1 in the mutant. Similarly, a change in the relative amplitude of the fast and slow components of $PhQ^{\bullet-}$ oxidation was observed in the PsaA-L722Y mutant, which cannot be fully accounted for by the charge recombination occurring in a fraction of PS I RCs. This suggests that the redistribution of kinetic phases also occurs in this mutant.

A relatively simple explanation for this apparently puzzling result lies in the occurrence of reversible electron transfer between PhQ_A, PhQ_B, and F_X as a result of the low driving force associated with these reactions. It was earlier proposed[2] that, in the case of small equilibrium constants for $PhQ^{\bullet-}$ oxidation by F_X, the order-of-magnitude difference in the experimentally determined *lifetimes* of $PhQ^{\bullet-}$ oxidation results from endergonic oxidation of $PhQ_A^{\bullet-}$ and exergonic oxidation of $PhQ_B^{\bullet-}$,[2] while the *actual rates* (and relative amplitudes) of electron transfer to F_X on both ET chains are substantially similar. This energetic asymmetry would make $PhQ_A^{\bullet-}$ a local thermodynamic trap so that a fraction of electrons are transferred from $PhQ_B^{\bullet-}$ to PhQ_A through F_X in a reaction path effectively resulting in interquinone ET. The observed amplitude of this kinetic component is expected to be small in optical measurements because it is weighted by a small extinction coefficient corresponding essentially to the difference between two chemically identical cofactors (PhQ_B and PhQ_A). If the PsaA-L722T mutation decreased the reduction potential of the $PhQ_A/PhQ_A^{\bullet-}$ couple, it would then increase the driving force for $PhQ_A^{\bullet-}$ oxidation and decrease the overall interquinone ET, with the net effect of redistributing the amplitude of the fast and slow kinetics of $PhQ^{\bullet-}$ oxidation. The apparent increase in the observed amplitude of the fast component, as well as the increase in the amount of $PhQ^{\bullet-}$ seen in the t_0 spectrum, would then stem from the larger differential extinction coefficient of $[PhQ_B^{\bullet-}F_X^- - PhQ_BF_X]$ compared to that of $[PhQ_B^{\bullet-}PhQ_A - PhQ_BPhQ_A^{\bullet-}]$.

Semiquantitative Description of Interquinone ET: Effects of the Mutations. A consequence of this "dynamic" equilibrium model is that the measured lifetimes will differ from the actual ET rates. This is a well-known problem in complex chemical kinetics because the observed lifetimes are linear combinations of the actual reaction rates and equilibrium constants. Still, in the absence of analytical solutions, the population dynamics of the cofactors of interest can be simulated numerically. To this aim, we have considered a simplified model taking into account only PhQ_A, PhQ_B, and F_X (Figure 5). Simulations resulting from this minimal model are not designed to describe quantitatively the ET dynamics within PS I, but rather, represent a qualitative tool to investigate the effects of the mutations, as an initial test of our hypothesis. Thus, for simplicity, the rate constants are computed assuming a common value for the reorganization energy, λ_t, so that the only adjustable parameter is $\Delta G^0_{PhQ^- \rightarrow F_x}$ accompanying $PhQ^{\bullet-}$ oxidation (Figure 5). The standard Gibbs free energy difference associated with F_X^- oxidation by F_A (although this cofactor is not explicitly included in the calculation) is derived from the published standard potential: $\Delta G^0_{F_X^- \rightarrow F_A} = -153$ meV.[2,37] Also, for the sake of simplicity, the initial populations of $PhQ_A^{\bullet-}$ and $PhQ_B^{\bullet-}$ were set to equal, while that of reduced F_X was set to zero. In this simulation, we consider that the edge-to-edge distance between $PhQ_{A/B}$ and F_X is not affected by the mutations. Moreover, this minimal model does not incorporate the "intermediate" kinetic phase with associated lifetime of 160−180 ns assigned to ET from F_X to F_A/F_B.[11,12] Even though this component was predicted in an extended modeling that included the terminal FeS clusters,[2] here, we limit discussion to the simpler three-stage model, since it is the redistribution of kinetic phases of $PhQ_A^{\bullet-}$ oxidation that we are principally trying to explain, and it is only semiquantitative information that we aim to retrieve.

The results of the calculations performed for the WT scenario are presented in Figure 5 (left panel). When the ΔG^0 of $PhQ_B^{\bullet-}$ and $PhQ_A^{\bullet-}$ oxidation are set to −25 and +10 meV, respectively, the simulated kinetics are described by three exponential decay components, which involve all the species considered, having lifetimes of 9.2, 23, and 261 ns (Figure 5). The first two components are likely too similar in rate to be experimentally resolved, so the experimentally observed "fast" phase would actually represent some form of weighted average of the two (Figure 5). The lifetime associated with the "slow" phase of $PhQ^{\bullet-}$ oxidation ($\tau_{exp} = 256 \pm 12$ ns) is reproduced sufficiently well by the simulations ($\tau_{sim} \approx 262$ ns).

An interesting observation is that, despite identical initial populations for $PhQ_A^{\bullet-}$ and $PhQ_B^{\bullet-}$ used in the calculations, the apparent proportion of the fast (sum of 10- and 23-ns components) and the slow component (262 ns) is 0.3:0.7, which agrees quite well with the experimental data (0.37:0.63; Table 1). Interestingly, the $PhQ_A^{\bullet-}$ population undergoes an initial (small) decrease, followed by a rise in concentration in the tens of nanoseconds (Figure 5, left panel). This is due to the effective transfer of electrons from $PhQ_B^{\bullet-}$ to PhQ_A, mediated by F_X.

To mimic the effect of the PsaA-L722T (and PsaA-L722Y) mutations, we considered two scenarios: one in which $PhQ_A^{\bullet-}$ oxidation by F_X is isoenergetic ($\Delta G^0 = 0$ meV) and one in which the reaction is slightly exergonic ($\Delta G^0 = -10$ meV), which are depicted in the center and right panels of Figure 5, respectively. Both scenarios reproduce qualitatively the experimentally observed acceleration of $PhQ^{\bullet-}$ oxidation. The calculated value of 187 ns for the apparent lifetimes obtained for the slightly exergonic case is closer to that observed experimentally (171 ± 10 ns) than the corresponding value from the isoenergetic model (~214 ns). Moreover, the apparent redistribution of the amplitude associated with "fast" and "slow" phases is well reproduced in the simulations. The fractional amplitudes of the 10-ns and 180-ns phases are 0.37:0.63 and 0.45:0.55 for the isoenergetic and the slightly exergonic scenarios, respectively. The change in amplitude of the ~20-ns and ~250-ns kinetic components is associated with the suppression of the rise phase in the ~10−40 ns interval in the $[P_{700}^+PhQ_A^{\bullet-}]$ radical pair. By increasing the driving force of ET from $PhQ_A^{\bullet-}$ to F_X, net interquinone ET becomes less favorable so that the relative amplitudes measured in these cases reflect more closely the actual relative utilization of the A- and B-branches (i.e., 1:1 in this scenario). Such figures are in close agreement with those obtained from studying charge recombination at 100 K after suppression of forward ET from $PhQ^{\bullet-}$ to F_X (0.45:0.55;[6,7]).

To mimic the PsaB-L706Y mutation, we repeated the simulation after increasing the driving force for $PhQ_B^{\bullet-}$ oxidation (Figure 6, left panel). The standard midpoint potential was increased by 40 meV. This value represents the minimal perturbation that qualitatively reproduced the effect of this mutation. It results in a shortening of all three lifetimes to values of 9.3, 13, and 231 ns. The last lifetime, which is commonly discussed as being associated principally with the oxidation of $PhQ_A^{\bullet-}$, becomes shorter with respect to the WT, and this reproduces a puzzling feature of the experimental results. Hence, it is unnecessary to invoke "indirect effects" of the mutation to

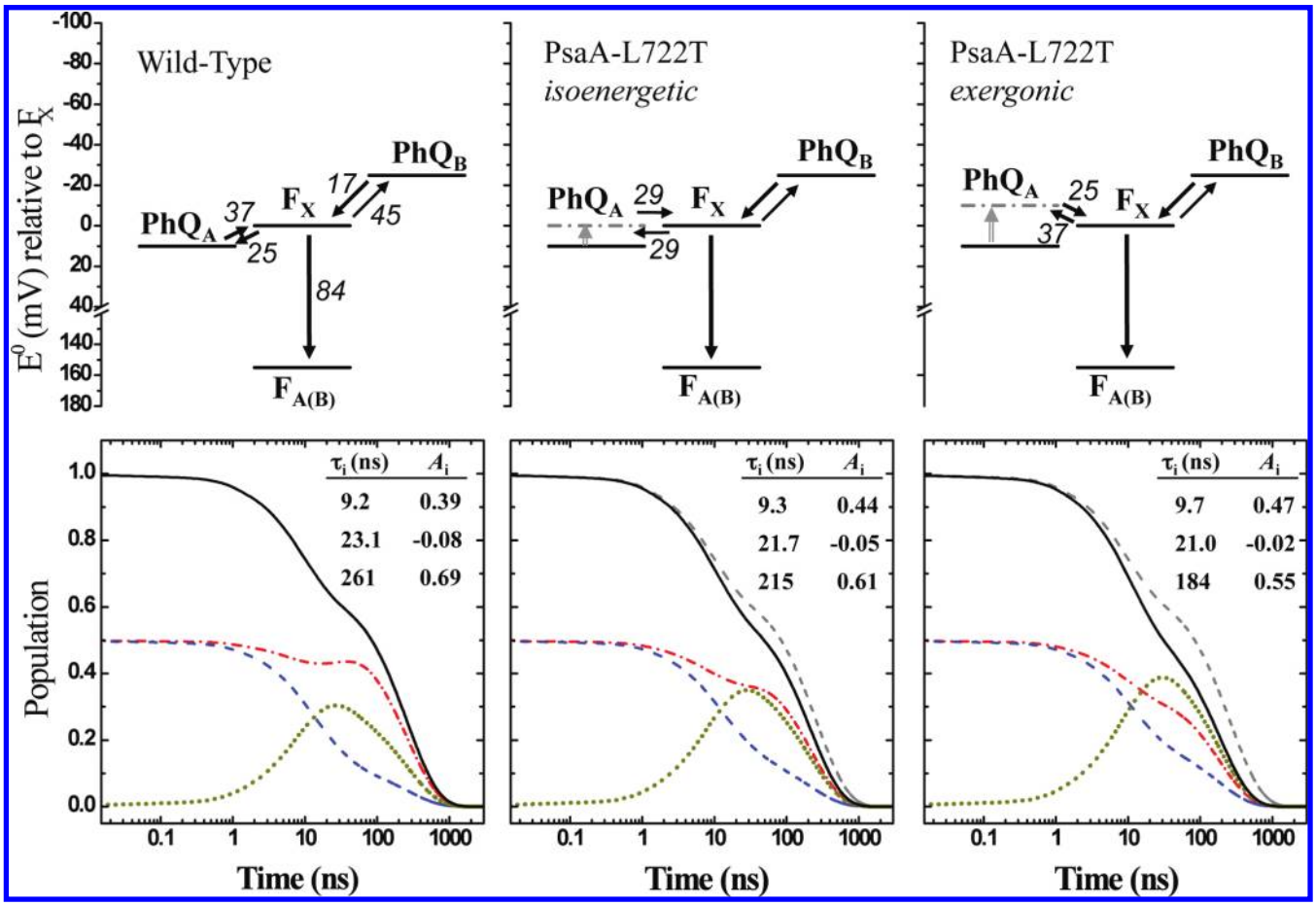

Figure 5. Schematic representation of the energetics of $PhQ^{\bullet-}$ oxidation and resulting simulation of population evolution in three cases: WT, PsaA-L722T (isoenergetic scenario), and PsaA-L722T (exergonic scenario). The dashed gray lines in the latter panels are the simulation of total $PhQ^{\bullet-}$ population evolution for the WT to allow direct comparison. Energetic Schemes: black solid lines, WT levels; dashed-gray lines show the suggested mutation-induced shift of standard midpoint potentials. The black arrows show the ET reactions included in the simulations; also shown are the *inverse* values of the calculated rate constants (units of ns). Kinetic simulations: population evolution of total $PhQ^{\bullet-}$ (solid black lines), $PhQ_A^{\bullet-}$ (dashed red line), $PhQ_B^{\bullet-}$ (dashed blue line), and F_X (dashed−dotted golden lines). The dashed gray line is total $PhQ^{\bullet-}$ in the WT. Also shown are simulated observable lifetimes (τ_i) and relative amplitudes (A_i) for the total $PhQ^{\bullet-}$ population. Simulation parameters: ΔG^0 ($= -F\Delta E^0$) is shown in the scaled energetic diagrams (upper panels); the donor−acceptor distances (X_{DA}) are taken from re 13). The values of electronic coupling elements, calculated as described in the material and methods, are: $|V_{PhQ_AF_x}||V_{PhQ_BF_x}| = 9.3 \times 10^{-4}$ eV, $|V_{F_XF_A}| = 1.5 \times 10^{-4}$ eV. Simulations were performed assuming a communal value of $\lambda_t = 0.675$ eV and coupling with a (communal) mean mode of energy $\hbar\bar{\omega} = k_bT = 25$ meV.

explain the acceleration of the ~250-ns phase in the PsaB-L706Y strain to ~200 ns. For a relatively moderate increase of the free energy of $PhQ_B^{\bullet-}$ oxidation, the more rapid oxidation kinetics of $PhQ^{\bullet-}$ results predominantly from the acceleration of the 24-ns component in the WT to 13 ns in the simulated kinetics for this mutant. The relative intensity of the F_X-mediated population transfer from $PhQ_B^{\bullet-}$ to $PhQ_A^{\bullet-}$ is increased in the PsaB-L706Y scenario, as expected for an effective increase in free energy for the overall ET reaction. As a consequence, a slight redistribution in the apparent amplitude of the $PhQ^{\bullet-}$oxidation phases in favor of the faster component is predicted (0.35:0.65, as compared to 0.29:0.71 in the WT). This is in apparent contradiction with the experimental results, in which the amplitude of the fast phase is decreased. However, as previously discussed, the measured amplitudes were, in this particular case, biased by insufficient time resolution of the spectrometer. Consistent with this, in the simulation, the total $PhQ^{\bullet-}$ population (i.e., sum of $PhQ_A^{\bullet-}$ and $PhQ_B^{\bullet-}$) at $t = 5$ ns would be decreased by ~25% in the PsaB-L706Y mutant (Figure 6). Thus, considering that the acceleration of the modeled lifetimes to 9.7 and 13 ns in this mutant likely represents an underestimation and, since the amplitude of faster decay components in the PsaB-L708Y is probably underestimated because of insufficient temporal resolution, it can be concluded that the simulation provides a qualitative explanation for our experimental observations.

Finally, to validate our model, we have also performed simulations aimed at describing the PsaA-W693F mutant, which had been previously characterized.[4] In this strain, the lifetime of the "slow" phase of $PhQ^{\bullet-}$ oxidation was lengthened to ~450 ns, while the fast component was virtually unaffected by the mutation. The relative amplitudes of the two oxidation phases were not much modified.[4] Assuming that the deceleration of the slower $PhQ^{\bullet-}$oxidation phase is the result of reducing the driving force of the $PhQ_A^{\bullet-}$ oxidation, we performed simulations in which $\Delta G^0_{PhQ_A^- \rightarrow F_X}$ was increased by 25 meV (Figure 6, right panel). The lifetimes calculated for this scenario are 8.7, 24, and 431 ns, which are comparable to the experimental results. The ratio of the amplitude of the rapid to the slow phase of $PhQ^{\bullet-}$ oxidation is calculated to become 0.22:0.78 in the mutant, as compared to 0.29:0.71 in the WT. This corresponds to a ~10% phase redistribution, which, although small, would appear to slightly exceed the value determined experimentally. Still, it is worth noticing that the alteration in amplitude predicted for the PsaA-W693F mutation is significantly less pronounced than what was predicted for the PsaA-L722T mutation (Figure 5).

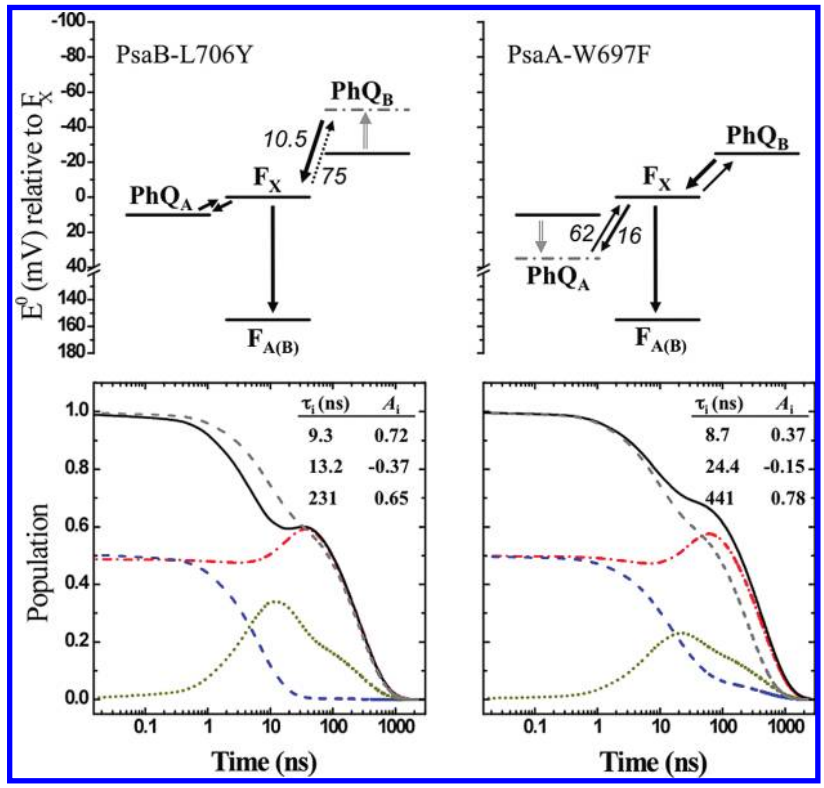

Figure 6. Schematic representation of the energetics of $PhQ^{\bullet-}$ oxidation and resulting simulation of population evolution in the PsaB-L706Y and PsaA-W693F mutants. See legend to Figure 5 for details.

The relative amplitudes are thus predicted to be more sensitive to an acceleration of ET from PhQ_A to F_X than to a deceleration, which likely explains why this effect was not noticed until now. A much larger increase of $\Delta G^0_{PhQ_A^- \rightarrow F_x}$ would be expected to have a larger, and much more easily observed, apparent redistribution of phases.

Considering the number of constraints employed in the kinetic model, including the oversimplification of imposing a communal value of the reorganization energy for all the ET reactions and its invariance upon specific amino acid substitutions, we think that the overall description of the experimental results, in terms of weakening of the H-bond to PhQ_A as a result of the substitution at PsaA-Leu722, is satisfactory overall. Nevertheless, it is worth emphasizing that we have no direct evidence for perturbation of the H-bond to PhQ_A. There seems to be a gradient of effects of substitution at position 722 of PsaA in *C. reinhardtii*: the largest side chain (Trp) seems to disturb the stability of PS I so profoundly that very little can accumulate; the smaller Tyr allows more assembly and results in some empty (or double-reduced) sites, with the PhQ-occupied sites displaying faster ET-to-F_X; the smaller β-branched Thr allows normal accumulation of PS I with fully active PhQ_A sites that display faster ET kinetics. It may be that mutation-induced structural rearrangements cause an acceleration of the forward ET reaction for other reasons in addition to changes in H-bonding (e.g., a decrease in reorganization energy). In this context, however, it is worth noting that every mutation made to the PhQ_A site until this time (e.g., PsaA-W697F,[4] PsaA-W697L,[47] PsaA-E699Q,[4] PsaA-S692A,[39] PsaA-G693W[39]) led to a *slowing* of ET from $PhQ_A^{\bullet-}$ to F_X, which would preclude the hypothesis that any gross structural perturbation could accelerate this reaction. Further investigations, including more direct observation of H-bonding to PhQ in the mutants investigated here, and perhaps novel side-chain substitutions of PsaA-Leu722 and PsaB-Leu706, may shed light on these issues.

Conclusion

An acceleration of the kinetics of oxidation of either $PhQ_A^{\bullet-}$ or $PhQ_B^{\bullet-}$ is observed in mutants of the conserved Leu residue involved in H-bonding to the respective quinone. These kinetic effects are interpreted in terms of a weakening of the H-bond to either PhQ_A or PhQ_B. This can be related to a shift toward a more negative reduction potential by ~20−40 mV, resulting from the destabilization of the $PhQ^{\bullet-}$ anion. Energetic asymmetry in the driving force of $PhQ_A^{\bullet-}$ (endergonic) and $PhQ_B^{\bullet-}$ (exergonic) oxidation by F_X, results in a "dynamic quasi-equilibrium" between the ET cofactors and, inevitably, to a F_X-mediated interquinone ET from $PhQ_B^{\bullet-}$ to PhQ_A. This process is, in principle, analogous to the direct one-electron reduction of Q_B by $Q_A^{\bullet-}$ in type II RCs, but has not been previously either observed or explicitly discussed for the case of type I RCs. However, although in type II RCs interquinone, ET leads to the metastable population of (protonated) semiquinonic (and quinolic) form of the acceptor, in the case of PS I, this represents only a transient process imposed by the low driving force associated with F_X reduction.

Acknowledgment. This study was funded in part by Energy Biosciences Grant DE-FG02-08ER15989 from the Department of Energy to K.R. Shannon Audley initiated the site-directed mutagenesis while funded as an NSF REU student at the University of Alabama. F.R. acknowledges financial support form the CNRS and UPMC. The work in Padua was supported by the Italian Ministry for University and Research (MURST) under project PRIN2007.

Supporting Information Available: 1. Growth tests of transformants in WT genetic background (Figure S1). 2. Quantitative immunoblots (anti-PsaA) of transformants (Figure S2 and Table S1). 3. Global deconvolution of FDMR spectra detected at 720 nm in thylakoids (a) incubated in the presence

of 11 mM dithionite at room temperature in the dark (Figure S3) and (b) preilluminated with 11 mM dithionite at room temperature (Figure S4). 4. Microwave-induced triplet-minus-singlet difference spectra recorded in thylakoids (Figure S5). 5. Details of the fitting of ET kinetics in the WT and mutants (Table S2). This material is available free of charge via the Internet at http://pubs.acs.org.

References and Notes

(1) Brettel, K.; Leibl, W.; Electron transfer in photosystem, I. *Biochim. Biophys. Acta-Bioenerg.* **2001**, *1507* (1−3), 100–114.

(2) Santabarbara, S.; Heathcote, P.; Evans, M. C. Modelling of the electron transfer reactions in Photosystem I by electron tunnelling theory: the phylloquinones bound to the PsaA and the PsaB reaction centre subunits of PS I are almost isoenergetic to the iron-sulfur cluster F(X). *Biochim. Biophys. Acta* **2005**, *1708* (3), 283–310.

(3) Srinivasan, N.; Golbeck, J. H. Protein-cofactor interactions in bioenergetic complexes: the role of the A1A and A1B phylloquinones in Photosystem I. *Biochim. Biophys. Acta* **2009**, *1787* (9), 1057–88.

(4) Guergova-Kuras, M.; Boudreaux, B.; Joliot, A.; Joliot, P.; Redding, K. Evidence for two active branches for electron transfer in photosystem I. *Proc. Natl. Acad. Sci. U.S.A.* **2001**, *98* (8), 4437–4442.

(5) Muhiuddin, I. P.; Heathcote, P.; Carter, S.; Purton, S.; Rigby, S. E. J.; Evans, M. C. W. Evidence from time resolved studies of the $P700^{\bullet+}$/$A1^{\bullet-}$ radical pair for photosynthetic electron transfer on both the PsaA and PsaB branches of the photosystem I reaction centre. *FEBS Lett.* **2001**, *503* (1), 56–60.

(6) Santabarbara, S.; Kuprov, I.; Fairclough, W. V.; Purton, S.; Hore, P. J.; Heathcote, P.; Evans, M. C. Bidirectional electron transfer in photosystem I, determination of two distances between P_{700}^{+} and A1- in spin-correlated radical pairs. *Biochemistry* **2005**, *44* (6), 2119–28.

(7) Santabarbara, S.; Kuprov, I.; Hore, P. J.; Casal, A.; Heathcote, P.; Evans, M. C. Analysis of the spin-polarized electron spin echo of the [P_{700}^{+} A^{1-}] radical pair of photosystem I indicates that both reaction center subunits are competent in electron transfer in cyanobacteria, green algae, and higher plants. *Biochemistry* **2006**, *45* (23), 7389–403.

(8) Bautista, J. A.; Rappaport, F.; Guergova-Kuras, M.; Cohen, R. O.; Golbeck, J. H.; Wang, J. Y.; Beal, D.; Diner, B. A. Biochemical and biophysical characterization of photosystem I from phytoene desaturase and zeta-carotene desaturase deletion mutants of *Synechocystis sp.* PCC 6803: Evidence for PsaA- and PsaB-side electron transport in cyanobacteria. *J. Biol. Chem.* **2005**, *280* (20), 20030–41.

(9) Poluektov, O. G.; Paschenko, S. V.; Utschig, L. M.; Lakshmi, K. V.; Thurnauer, M. C. Bidirectional electron transfer in photosystem I. direct evidence from high-frequency time-resolved EPR spectroscopy. *J. Am. Chem. Soc.* **2005**, *127* (34), 11910–1.

(10) Li, Y.; van der Est, A.; Lucas, M. G.; Ramesh, V. M.; Gu, F.; Petrenko, A.; Lin, S.; Webber, A. N.; Rappaport, F.; Redding, K. Directing electron transfer within Photosystem I by breaking H-bonds in the cofactor branches. *Proc. Natl. Acad. Sci. U.S.A.* **2006**, *103* (7), 2144–9.

(11) Byrdin, M.; Santabarbara, S.; Gu, F.; Fairclough, W. V.; Heathcote, P.; Redding, K.; Rappaport, F. Assignment of a kinetic component to electron transfer between iron−sulfur clusters F(X) and F(A/B) of Photosystem I. *Biochim. Biophys. Acta* **2006**, *1757* (11), 1529–38.

(12) Santabarbara, S.; Jasaitis, A.; Byrdin, M.; Gu, F.; Rappaport, F.; Redding, K. Additive effect of mutations affecting the rate of phylloquinone reoxidation and directionality of electron transfer within photosystem I. *Photochem. Photobiol.* **2008**, *84* (6), 1381–7.

(13) Jordan, P.; Fromme, P.; Witt, H. T.; Klukas, O.; Saenger, W.; Krauss, N. Three-dimensional structure of cyanobacterial photosystem I at 2.5 A resolution. *Nature* **2001**, *411* (6840), 909–17.

(14) Ben-Shem, A.; Frolow, F.; Nelson, N. Crystal structure of plant photosystem I. *Nature* **2003**, *426*, 630–5.

(15) Schlodder, E.; Falkenberg, K.; Gergeleit, M.; Brettel, K. Temperature dependence of forward and reverse electron transfer from A1−the reduced secondary electron acceptor in photosystem I. *Biochemistry* **1998**, *37* (26), 9466–76.

(16) Agalarov, R.; Brettel, K. Temperature dependence of biphasic forward electron transfer from the phylloquinone(s) A(1) in photosystem I: only the slower phase is activated. *Biochim. Biophys. Acta* **2003**, *1604* (1), 7–12.

(17) Ishikita, H.; Knapp, E. W. Redox potential of quinones in both electron transfer branches of photosystem I. *J. Biol. Chem.* 2003.

(18) Karyagina, I.; Pushkar, Y.; Stehlik, D.; van der Est, A.; Ishikita, H.; Knapp, E. W.; Jagannathan, B.; Agalarov, R.; Golbeck, J. H. Contributions of the protein environment to the midpoint potentials of the A1 phylloquinones and the Fx iron-sulfur cluster in photosystem I. *Biochemistry* **2007**, *46* (38), 10804–16.

(19) Munge, B.; Das, S. K.; Ilagan, R.; Pendon, Z.; Yang, J.; Frank, H. A.; Rusling, J. F. Electron transfer reactions of redox cofactors in spinach photosystem I reaction center protein in lipid films on electrodes. *J. Am. Chem. Soc.* **2003**, *125* (41), 12457–63.

(20) Moser, C. C.; Dutton, P. L. Application of Marcus Theory to Photosystem I Electron Transfer. In *Photosystem I: The Plastocyanin: Ferredoxin Oxidoreductase in Photosynthesis*; Golbeck, J., Ed.; Kluwer Academic Publishers: Dordrecht, 2006; pp 583−594.

(21) Srinivasan, N.; Karyagina, I.; Bittl, R.; van der Est, A.; Golbeck, J. H. Role of the hydrogen bond from Leu722 to the A1A phylloquinone in photosystem I. *Biochemistry* **2009**, *48* (15), 3315–24.

(22) Li, Y.; Lucas, M.-G.; Konovalova, T.; Abbott, B.; MacMillan, F.; Petrenko, A.; Sivakumar, V.; Wang, R.; Hastings, G.; Gu, F.; van Tol, J.; Brunel, L.-C.; Timkovich, R.; Rappaport, F.; Redding, K. Mutation of the Putative Hydrogen-Bond Donor to P700 of Photosystem I. *Biochemistry* **2004**, *43* (39), 12634–12647.

(23) Redding, K.; MacMillan, F.; Leibl, W.; Brettel, K.; Rutherford, A. W.; Breton. J.; Rochaix, J.-D. A survey of conserved histidines in the photosystem 1: Methodology and analysis of the PsaB-H656L mutant. In *Photosynthesis: Mechanisms and Effects*; Garab, G., Ed.; Kluwer Academic Publishers: Dordrecht, 1998; Vol. 1; pp591−594.

(24) Harris, E. H. *The Chlamydomonas sourcebook. A comprehensive guide to biology and laboratory use*; Academic Press: San Diego, 1989; p 780.

(25) Santabarbara, S.; Agostini, G.; Casazza, A. P.; Syme, C. D.; Heathcote, P.; Bohles, F.; Evans, M. C.; Jennings, R. C.; Carbonera, D. Chlorophyll triplet states associated with Photosystem I and Photosystem II in thylakoids of the green alga Chlamydomonas reinhardtii. *Biochim. Biophys. Acta* **2007**, *1767* (1), 88–105.

(26) Béal, D.; Rappaport, F.; Joliot, P. A new high-sensitivity 10-ns time-resolution spectrophotometric technique adapted to in vivo analysis of the photosynthetic apparatus. *Rev. Sci. Instrum.* **1999**, *70*, 202–7.

(27) Carbonera, D.; Giacometti, G.; Agostini, G. FDMR of Carotenoids and Chlorophyll in Light-harvesting Complex II of Spinach. *Appl. Magn. Reson.* **1992**, *3*, 859–872.

(28) Carbonera, D.; Collareta, P.; Giacometti, G. The P700 triplet state in an intact environment detected by ODMR. A well resolved triplet minus singlet spectrum. *Biochim. Biophys. Acta* **1997**, *1322* (2−3), 115–128.

(29) Santabarbara, S.; Bordignon, E.; Jennings, R. C.; Carbonera, D. Chlorophyll triplet states associated with photosystem II of thylakoids. *Biochemistry* **2002**, *41* (25), 8184–94.

(30) Marcus, R.; Sutin, N. Electron transfers in chemistry and biology. *Biochim. Biophys. Acta* **1985**, *811* (3), 265–322.

(31) DeVault, D. *Quantum-Mechanical Tunnelling in Biological Systems*; Cambridge University Press: Cambridge, 1984.

(32) Hopfield, J. J. Electron Transfer Between Biological Molecules by Thermally Activated Tunneling. *Proc. Natl. Acad. Sci. U.S.A.* **1974**, *71* (9), 3640–3644.

(33) Moser, C. C.; Keske, J. M.; Warncke, K.; Farid, R. S.; Dutton, P. L. Nature of biological electron transfer. *Nature* **1992**, *355* (6363), 796–802.

(34) Redding, K.; MacMillan, F.; Leibl, W.; Brettel, K.; Hanley, J.; Rutherford, A. W.; Breton, J.; Rochaix, J. D. A systematic survey of conserved histidines in the core subunits of Photosystem I by site-directed mutagenesis reveals the likely axial ligands of P700. *EMBO J.* **1998**, *17* (1), 50–60.

(35) Ramesh, V. M.; Guergova-Kuras, M.; Joliot, P.; Webber, A. N. Electron transfer from plastocyanin to the photosystem I reaction center in mutants with increased potential of the primary donor in *Chlamydomonas reinhardtii*. *Biochemistry* **2002**, *41* (50), 14652–14658.

(36) Santabarbara, S.; Redding, K. E.; Rappaport, F. Temperature dependence of the reduction of P_{700}^{+} by tightly bound plastocyanin in vivo. *Biochemistry* **2009**, *48* (43), 10457–66.

(37) Brettel, K. Electron transfer and arrangement of the redox cofactors in photosystem I. *Biochim. Biophys. Acta* **1997**, *1318*, 322–373.

(38) Searle, G.; Schaafsma, T. Fluorescence Detected Magnetic Resonance of the Primary Donor and Inner Antenna Chlorophylls in Photosystem I Reaction Centres Proteins: Sign Inversion and Energy Transfer. *Photosyn. Res.* **1992**, *32*, 193–206.

(39) Rappaport, F.; Diner, B. A.; Redding, K. Optical measurements of secondary electron transfer in Photosystem I. In *Photosystem I: The Plastocyanin:Ferredoxin Oxidoreductase in Photosynthesis*; Golbeck, J., Ed.; Kluwer Academic Publishers: Dordrecht, 2006; pp 223−244.

(40) Redding, K.; van der Est, A.; The Directionality of Electron Transfer in Photosystem I In *Photosystem I: The Plastocyanin:Ferredoxin Oxidoreductase in Photosynthesis*; Golbeck, J., Ed.; Kluwer Academic Publishers: Dordrecht, 2006; pp 413−437.

(41) Xu, W.; Chitnis, P. R.; Valieva, A.; van der Est, A.; Brettel, K.; Guergova-Kuras, M.; Pushkar, Y. N.; Zech, S. G.; Stehlik, D.; Shen, G.; Zybailov, B.; Golbeck, J. H. Electron transfer in cyanobacterial photosystem I: II Determination of forward electron transfer rates of site-directed mutants in a putative electron transfer pathway from A0 through A1 to FX. *J. Biol. Chem.* **2003**, *278* (30), 27876–87.

(42) Ali, K.; Santabarbara, S.; Heathcote, P.; Evans, M. C.; Purton, S. Bidirectional electron transfer in photosystem I replacement of the sym-

metry-breaking tryptophan close to the PsaB-bound phylloquinone A1B with a glycine residue alters the redox properties of A1B and blocks forward electron transfer at cryogenic temperatures. *Biochim. Biophys. Acta* **2006**, *1757* (12), 1623–33.

(43) Müller, M. G.; Niklas, J.; Lubitz, W.; Holzwarth, A. R. Ultrafast transient absoprtion studies on photosystem I reaction centers from *Chlamydomonas reinhardtii* I. A new interpretation of the energy trapping and early electron transfer steps in photosystem I. *Biophys. J.* **2003**, *85* (6), 3899–3922.

(44) Müller, M. G.; Slavov, C.; Luthra, R.; Redding, K. E.; Holzwarth, A. R. Independent initiation of primary electron transfer in the two branches of the photosystem I reaction center. *Proc. Natl. Acad. Sci. U.S.A.* **2010**, *107* (9), 4123–8.

(45) Srinivasan, N.; Karyagina, I.; Golbeck, J. H.; Stehlik, D., Structure-Function Correlations in the (A0 → A1 → FX) Electron Transfer Kinetics of the Phylloquinone (A1) Acceptor in Cyanobacterial Photosystem I. In *Photosynthesis. Energy from the Sun: 14th International Congress on Photosynthesis*; Allen, J. F.; Gantt, E.; Golbeck, J. H.; Osmond, B., Eds.; Springer: Dordrecht, The Netherlands, 2007; pp 207−210.

(46) Nakamura, A.; Watanabe, T. Separation and determination of minor photosynthetic pigments by reversed-phase HPLC with minimal alteration of chlorophylls. *Anal. Sci.* **2001**, *17* (4), 503–8.

(47) Fairclough, W. V.; Forsyth, A.; Evans, M. C.; Rigby, S. E.; Purton, S.; Heathcote, P. Bidirectional electron transfer in photosystem I electron transfer on the PsaA side is not essential for phototrophic growth in Chlamydomonas. *Biochim. Biophys. Acta* **2003**, *1606* (1−3), 43–55.

JP1038656